Exploiting sulfonated covalent organic frameworks to fabricate long-lasting stability and chlorine-resistant thin-film nanocomposite nanofiltration membrane

Check for updates

Wenqiao Meng[1,2], Qiang Xue[1,2], Jinyuan Zhu[1,2] & Kaisong Zhang [ID][3,4] ✉

Incorporating hydrophilic and charged porous nanofillers to prepare high-performance thin film nanocomposite (TFN) nanofiltration (NF) membranes is an effective method to achieve efficient water treatment. In this study, we synthesize the sulfonated covalent organic framework nanosheets (S-CONs) with higher hydrophilicity and electronegativity by immobilizing sulfonic acid groups ($-SO_3H$) on TpPa-1 nanosheets. The S-CONs are incorporated in the PA layer by interfacial polymerization (IP) reaction. The results indicated that the S-CONs could modulate the hydrophilicity, thickness, and electronegativity of TFN-NF membranes. At the optimal addition of S-CONs (0.006 g), the pure water permeance increases to $8.84 \, L \cdot m^{-2} \cdot h^{-1} \cdot bar^{-1}$, which is about 1.75 times than the TFC membrane, with a high Na_2SO_4 rejection reaching 98.97%. The improvement of the separation performance mainly results from the reduction of PA layer thickness (from ~178.00–198.00 to ~100.00–128.00 nm) and the increase of surface electronegativity (from -20.37 to -44.41 mV at pH = 7.00). More interestingly, the amide bond formed between the S-CONs and TMC improved the chlorine resistance of the membranes. This study reveals the potential of using functionalized 2D CONs as nanofillers to modify TFC membranes for efficient nanofiltration.

Membrane technology is a promising solution that has been developed in recent years to address freshwater shortage and pollution problems[1]. Nanofiltration (NF) is a low-energy water treatment technology for the removal of divalent ions from water based on size and charge exclusion effects[2,3] with separation accuracy in the range of 0.50–2.00 nm[4]. TFC-NF membrane is the core component of nanofiltration technology, which is synthesized by the interfacial polymerization (IP) reaction of piperazine (PIP) with 1,3,5-Trichlorobenzoylchloride (TMC) on a porous ultrafiltration (UF) substrate. However, the perm-selectivity trade-off remains a bottleneck for further development of TFC nanofiltration[5]. Since Jeong et al.[6] proposed the modification of TFC by dispersing NaA zeolite nanoparticles in a polyamide layer in 2007, researchers have found that incorporating most of the nanomaterials (e.g., graphene oxide (GO)[7], MoS_2[8], and quantum dots[9]) into the PA layers could increase the water transport channel and the effective filtration area of the membrane, thereby enhancing

the water permeance and breaking the inherent limitations[10]. The membranes prepared by this method are named thin-film nanocomposite (TFN) membranes. It also has been discovered that the addition of nanomaterials helps to improve the membrane's anti-fouling performances and chemical durability (e.g., acid/alkaline resistance and chlorine resistance)[11–13]. Zhao et al.[14] introduced MWCNTs into the PA structure and found that the TFN membrane had enhanced hydrophilicity and increased negative surface charge, which led to improved antifouling properties. Moreover, the electron-rich MWCNTs protected the active sites in the PA layer from free chlorine attachment, thus improving the chlorine resistance of the TFN membrane. Liu et al.[15] prepared a hollow fiber (HF) TFN membrane with a water permeance of $14.30 \, L \cdot m^{-2} \cdot h^{-1} \cdot bar^{-1}$ by adding MoS_2 nanosheets into the PA layer. Meanwhile, it was also found that the high electronegativity of the membrane surface could not only realize high selective separation but also effectively prevent the contact between active chlorine

and the membrane surface, thus preventing the active chlorine from destroying the PA layer, which has better chlorine resistance. However, some of these inorganic nanomaterials may suffer from severe agglomeration and poor chemical compatibility with the PA selective layer, resulting in undesirable permeance (pore blockage or increased thickness) and selectivity (generation of non-selective voids or defects)[16]. Consequently, breaking through these limitations is the key to preparing high-performance TFN membranes.

As an emerging 2D nano-porous material, the pure organic covalent bond structure enables COFs better compatibility with PA layer[17] and offers tremendous advantages over classical inorganic nanomaterials in the preparation of TFN-NF membranes[18]. More significantly, the inherent pores of covalent organic frameworks nanosheets (CONs) can provide nanochannels for rapid water permeate[19]. Wang et al.[20] prepared PA-SNW-1/PES membranes with Na_2SO_4 rejection above 80.00% by dispersing COFs (SNW-1) in the aqueous phase, which exhibited long-term (70 h) operational stability. Khan et al.[21] incorporate CTN in the PA matrix, the synthesized PA-CTN TFC membrane exhibited higher hydrophilicity and better antifouling properties with Na_2SO_4 rejection above 95%. In our previous experiment[22], we prepared TpPa-1 COFs nanosheet (CONs) TFN-NF membranes with superior separation performance (pure water permeance up to $8.84 \, L \cdot m^{-2} \cdot h^{-1} \cdot bar^{-1}$ and Na_2SO_4 rejection reached 98.10%) and excellent long-lasting operation stability (35-day) than the TFC-NF membranes. The main reasons for the excellent performance of TFN in these studies include: (1) The suitable pore size and higher porosity of COFs, and the nano-pores formed between COFs and polyamides provided additional nanochannels for water molecules; (2) The incorporation of COFs modulates the roughness of the membrane surface, provided additional sites for membrane-water contact; (3) COFs increased the hydrophilicity of the membrane surface and reduced the mass transfer resistance, all of which contributed to improving the water permeance. The effect of COFs on the degree of cross-linking of the PA layer helped to sharpen the pore size distribution and improve the size effect of the TFN membranes. The charge groups carried by COFs increased the electronegativity of the TFN membrane surface, which enhanced Donnan rejection of multivalent anions. In addition, COFs were covalently linked with the PA matrix via the reaction between the -NH groups and the -COCl groups of TMC, which ensured membrane stability.

However, the NF separation processes are always affected by the combination of chemical-, charge- and size-based interactions[23]. We found that the enhancement of membrane surface properties was limited by relying only on the hydrolysis of the unreacted acyl chloride (–COCl) groups to generate carboxyl (–COOH) groups and the oxygen-containing functional groups carried by TpPa-1 CONs[24]. Therefore, a more hydrophilic and more strongly charge-negative porous nanomaterial is needed to strengthen the TFN-NF membrane separation performance. In recent years, researchers have found that charged functional groups (e.g., hydroxyl (–OH), carboxyl (–COOH)[25], and sulfonic acid groups (–SO_3H)[26]) on the nanomaterials would synergistically regulate the hydrophilicity and anion rejection of the NF membranes[27–30]. Zhu et al.[29] incorporated sulfonated MoS_2 nanosheets as nanofillers into the PA layer to construct a thinner and more hydrophilic selective layer, which resulted in the high separation and antifouling performance of the TFN membrane. Xue et al.[31] explored the effects of carboxyl-, hydroxyl- and amino-functionalized MWCNTs on the TFN performance. As for functional COFs, Xu et al.[23] prepared an efficient TFN-FO membrane by doping hydrophilic COF–COOH into the PA layer, the abundance of –COOH groups in COF–COOH results in increased hydrophilicity and electronegativity of the PA layer. This indicates that functionalized COFs are expected to play an important role in the preparation of TFN-NF modification.

Inspired by the above efforts, we propose to prepare sulfonated CONs (S-CONs) modified TFN-NF membranes. Compared with TpPa-1 CONs, the abundant –SO_3H groups of S-CONs ensure great potential for further modification to achieve the tailored design of TFN membrane[32]. As for the preparation of S-CONs, different from the post-modified methods of

loading sulfonic acid groups on MoS_2 by heat treatment[29], we chose the sulfonated amine monomer (Pa-SO_3H) to prepare S-COFs, which could ensure the uniform distribution of –SO_3H groups. As for the preparation of TFN-NF membranes, we chose to disperse the S-CONs in the organic phase and then embed them into the PA layer by IP reaction. In this way, the sulfonated nanosheets will be embedded in the upper part of the PA layer either flatly or tiltedly under the effect of their own gravity and chemical covalent bonding (formed by the reaction between TMC and S-CONs)[33]. Meanwhile, compared with dispersion in the aqueous phase, dispersion in the organic phase could make full utilization of the inherent hydrophilicity, electronegativity, and nano-pore of the S-CONs[34,35].

In this study, we investigated the effects of S-CONs on the membrane physicochemical properties, separation performance, long-lasting stability, and anti-fouling performance of the TFN-NF membranes compared to those of the pristine TFC membrane comprehensively. Moreover, we explored the interactions between the S-CONs and the PA layer by FTIR and XPS characterization and found that the covalent bonds were conducive to improve the chlorine resistance of the TFN-NF membranes. It provides an idea for organic nanofillers to modify TFC membranes and a feasible way for saline wastewater separation and treatment.

Results and discussion
Characterization of S-CONs
In this work, S-COFs were obtained by solvothermal synthesis, and the chemical and 3D structure of the S-COFs were given in Supplementary Fig. 1. Then, the S-CONs were exfoliated by mechanical grinding. It has been reported in the literature that the mechanical grinding method only increases the aspect ratio of nanomaterials without changing their crystal structure[36].

Both SEM (Fig. 1a) and TEM (Fig. 1b) results observed that the prepared S-CONs show a good lamellar structure with a rough surface. EDX demonstrated that the main element component of S-CONs was C, N, O, S (Fig. 1c). The disappearance and appearance of the peaks in ATR-FTIR (Fig. 1d) indicated the successful synthesis of TpPa-SO_3H COFs (S-COFs). The magnified images further demonstrated that the chemical structure of S-CONs has not changed after exfoliation. The XPS (Fig. 1e) further confirmed that S-CONs consists of C, N, O, S. The C1s, O1s, S2p of S-CONs and S-COFs were given in Supplementary Fig. 2. The P-XRD (Fig. 1f) observed the crystal structure of the nanosheets, the diffraction peaks around 5°, 14°, and 26°correspond to 100, 010, and 001 planes, respectively. It reaffirmed the successful synthesis and that the mechanical grinding method did not change their crystal structure.

AFM tested the thickness of S-CONs at around 1.35–1.57 nm (Fig. 2a), which is much thinner than the thickness of S-COFs (~7.25 nm, Supplementary Fig. 3a). ZetaPALS measured the zeta-potential of S-CONs at pH = 2.00–10.00 (Fig. 2b) and the particle lateral size distribution in n-hexane (Fig. 2c). Compared with S-COFs (Supplementary Fig. 3b), S-CONs have stronger electronegativity of −45.20 mV at pH = 7.00, while S-COFs have only −40.70 mV. The particle lateral size distribution of S-CONs ranged from 458.70 to 1106.00 nm (Supplementary Fig. 3c), with an average particle lateral size of ~578.00 nm, which is much smaller than that of S-COFs (particle lateral size distribution: 825.00–1484.00 nm, average particle lateral size: ~1083.00 nm). This implied that mechanical exfoliation can produce smaller nanosheets. The lateral size and thickness characteristics allow S-CONs to be better dispersed flat or inclined in the upper part of the PA layer[33,37].

The reaction between S-CONs and TMC was confirmed by FT-IR and XPS. A certain amount of S-CONs and TMC were added into the n-hexane and stirred at 400 rpm/min for 30 min. The powder was washed with n-hexane three times and dried in a vacuum oven at 60 °C for characterization. The FT-IR results showed the formation of amide bonds (N–C=O) at 1633 cm^{-1} (Fig. 2d)[17]. The XPS spectrum of N1s in Fig. 2e for the reaction powder could be divided into peaks at the binding energy of 397.81 and 401.51 eV, corresponding to the N–H and N–C=O, respectively[20]. These results indicated that S-CONs react with TMC to form covalent bonds
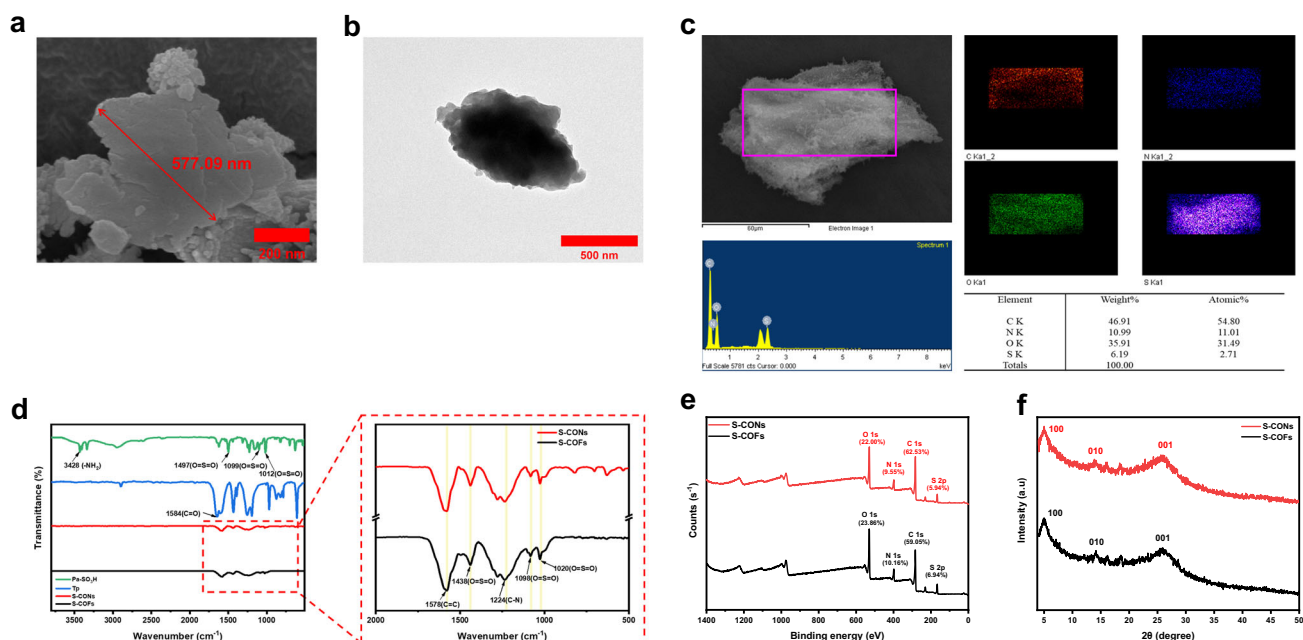
Fig. 1 | Characterization of S-CONs. a SEM image (scale bar 200 nm), **b** TEM image (scale bar 500 nm), **c** EDX image, **d** ATR-FTIR, **e** XPS, and **f** P-XRD.
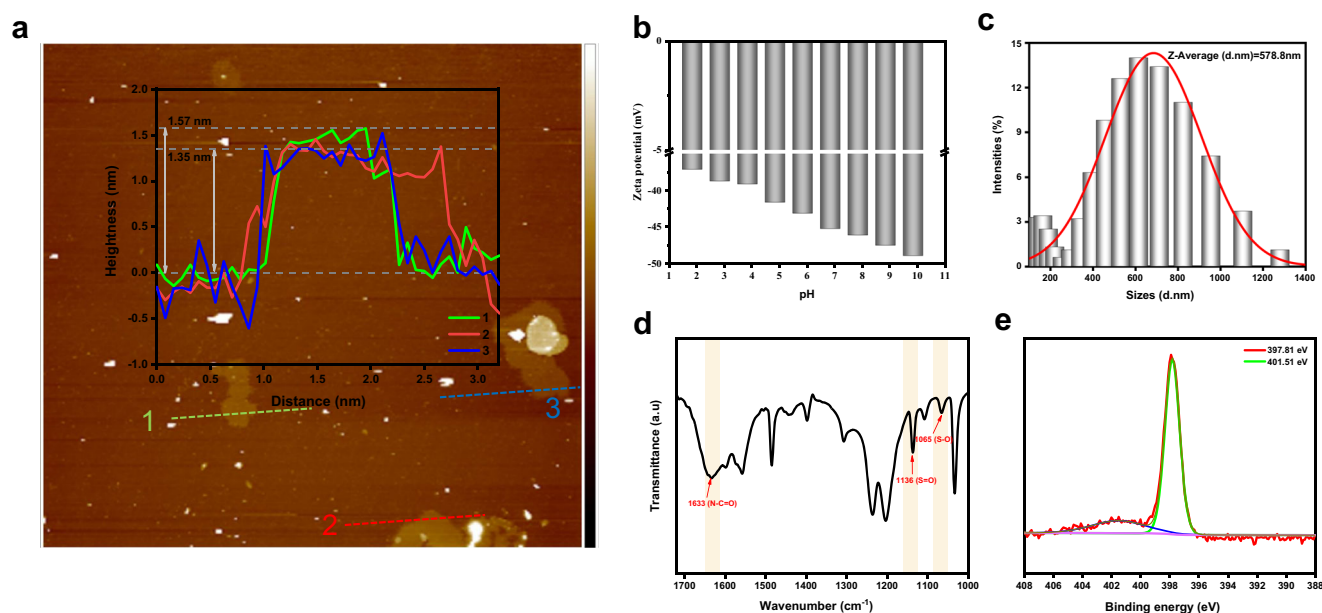

Fig. 2 | Characterization of S-CONs and its reaction with TMC. a AFM, **b** zeta-potential, **c** particle lateral size distribution, **d** FT-IR of the reaction, and **e** XPS of the reaction.

during the IP process. In addition, the nanosheets are also encapsulated by the PA layer formed during the IP process, which can be seen in SEM images (Supplementary Figs. 4, 5), allowing them to be better stabilized on the surface of the membrane[22]. Moreover, the covalent bonds could greatly enhance the compatibility and long-lasting stability of the membranes.

Characterization of S-CONs nanocomposite membrane

The influences of different S-CONs additions on the surface morphology of M1–M6 (which represent the addition amounts at 0.000, 0.004, 0.006, 0.007, 0.009, and 0.0100 g, respectively) were observed by FE-SEM. In Fig. 3a, the M1 (TFC) membrane illustrated a comparatively smooth surface with smaller spherically shaped bumps, which was a typical nodular structure formed by the reaction of PIP with TMC[38,39]. Figure 3b–d and

Supplementary Figs. 4, 5 exhibited a random distribution of S-CONs (marked with red dashed circles) on the M2–M6 (TFN) membrane surface. However, it should be noted that with the gradual increase of the addition amount, the S-CON aggregation occurs on the membrane surface. Therefore, it is necessary to avoid excessive aggregation by controlling the amount added.

The effects of S-CONs on the membrane's surface roughness were observed by AFM 3D scanning (5.00×5.00 μm, three randomly selected points, Fig. 3e, f, Supplementary Fig. 6 and Fig. 6). Supplementary Table 1 summarized the roughness parameters (mean roughness Ra and root mean square roughness Rq) of the membrane's surface. Owing to the distribution of S-CONs in the upper part of the PA layer, the surface roughness of the TFN membranes with S-CONs added was all higher than the TFC control
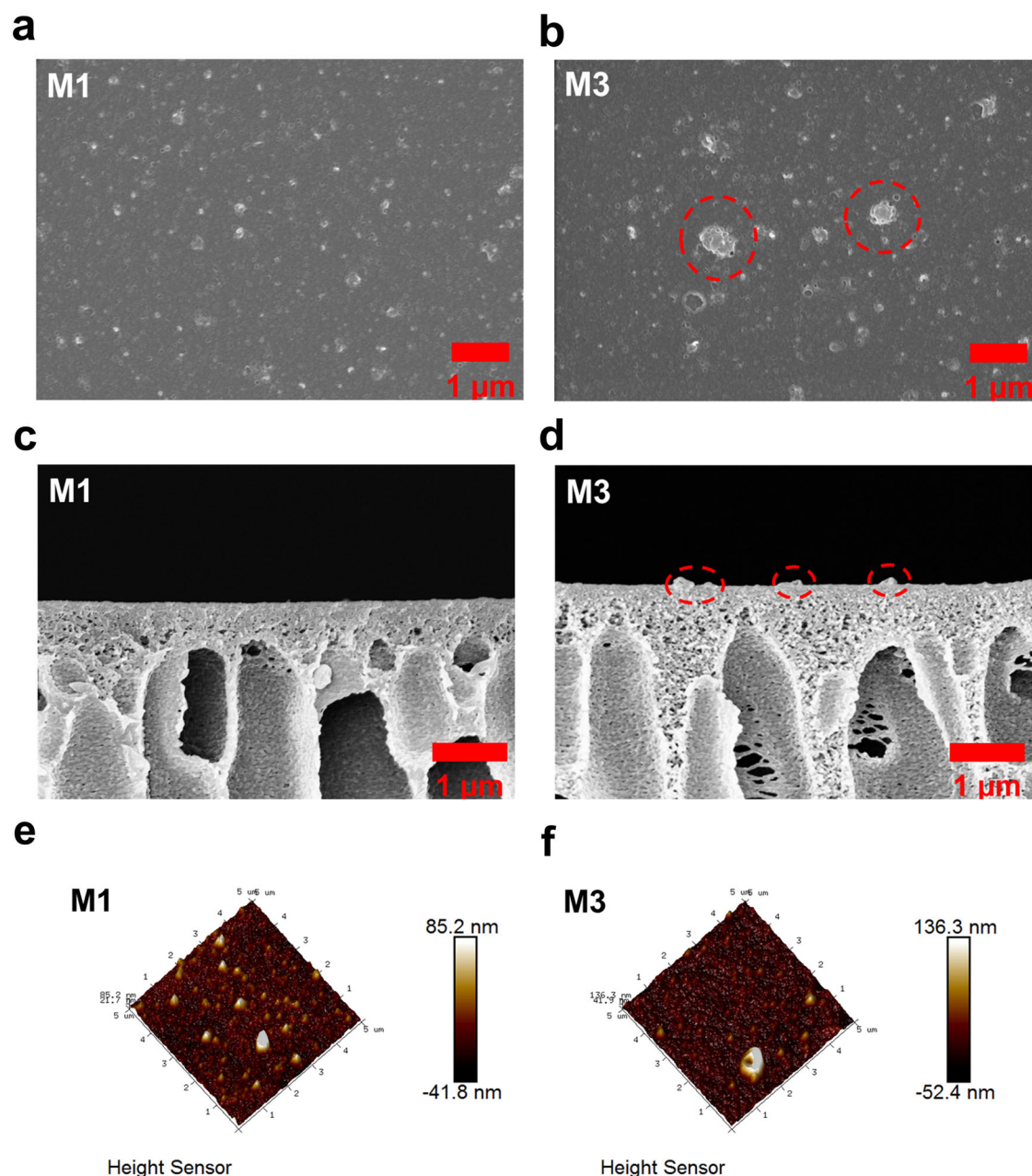
Fig. 3 | SEM and AFM characterization of M1 and M3. a and **b** the surface images of M1 and M3 (scale bar 1000 nm), **c** and **d** the cross-sectional images of M1 and M3 (scale bar 1000 nm), and **e** and **f** the AFM images of M1 and M3.

membrane (Ra = 10.60 ± 0.50 nm). And at the additional amount of 0.009 g, the surface roughness of M6 reached the maximum value (Ra = 26.60 ± 2.10 nm). In addition, the increased roughness not only implied that the nanosheets had been successfully anchored into the PA layer but also provided more contact area for water permeation, which facilitated the enhancement of membrane permeance[33,40,41]. However, excessive addition would lead to agglomeration in the membrane PA layer[42,43], as mentioned in the SEM images, thus resulting in the reduction of its salt rejection ability. Therefore, the optimal addition amount needs to be further determined by testing the membrane separation performance.

TEM further confirmed that the S-CONs were successfully embedded in TFN membranes (Fig. 4a, b), as indicated by the red arrow. Through the analysis of the PA layer thickness in the TEM image, it was found that the addition of S-CONs also contributed to the reduction of the PA layer thickness from ~178.00–198.00 to ~100.00–128.00 nm, which might facilitate reduce the solvent

transport pathway and allowed the membrane to have a higher permeance. The fluorescent qualities of the S-CONs can be characterized by LSCM in the green light field, as shown in Fig. 4c, d. The M1 did not show fluorescence, while M3 exhibited fluorescence, indicating the presence of the S-CONs. It is worth noting that the brightness and contrast of the image are mainly influenced by the flatness of the sample cross-section, independent of the specific distribution of the S-CONs. The presence of S elements in the M3 surface EDX (Fig. 4e) also validates the presence of nanosheets.

XPS is a sensitive technique for elemental composition measurement. In the full-scan spectrum (Fig. 5a), the characteristic peak of S $2p$ at 166.00 eV can be distinctly observed on the surface of M3, which also can be observed by EDX (Fig. 4e). Supplementary Table 1 demonstrates the element's composition on the surface of the prepared membrane. The content of elemental S on the TFN membrane surface gradually increases with the increase of S-CONs addition, indicating that more nanosheets are dispersed
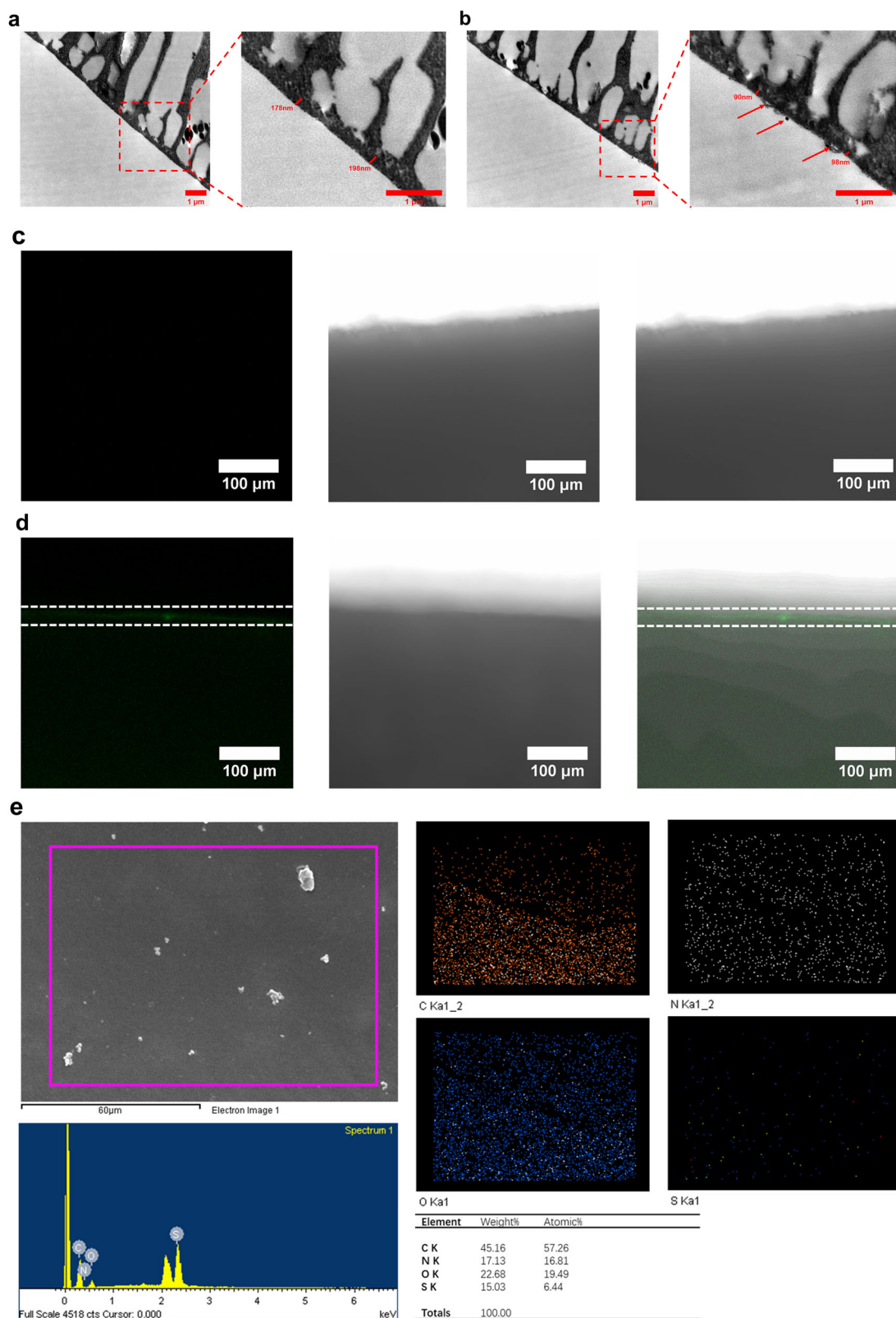
Fig. 4 | TEM, LSCM, and EDX characterization of the membranes. a and **b** the TEM images of M1 and M3 (The red arrow points to the S-CONs, scale bar 1000 nm), **c** and **d** the LSCM images of M1 and M3 (From top to bottom are the fluorescent images, bright-field images as well as superposed image of fluorescent images and bright-filed images, respectively. Between the red dashed lines are the measured PA layers containing fluorescent S-CONs, scale bar 100 μm), and **e** the EDX images of M3.
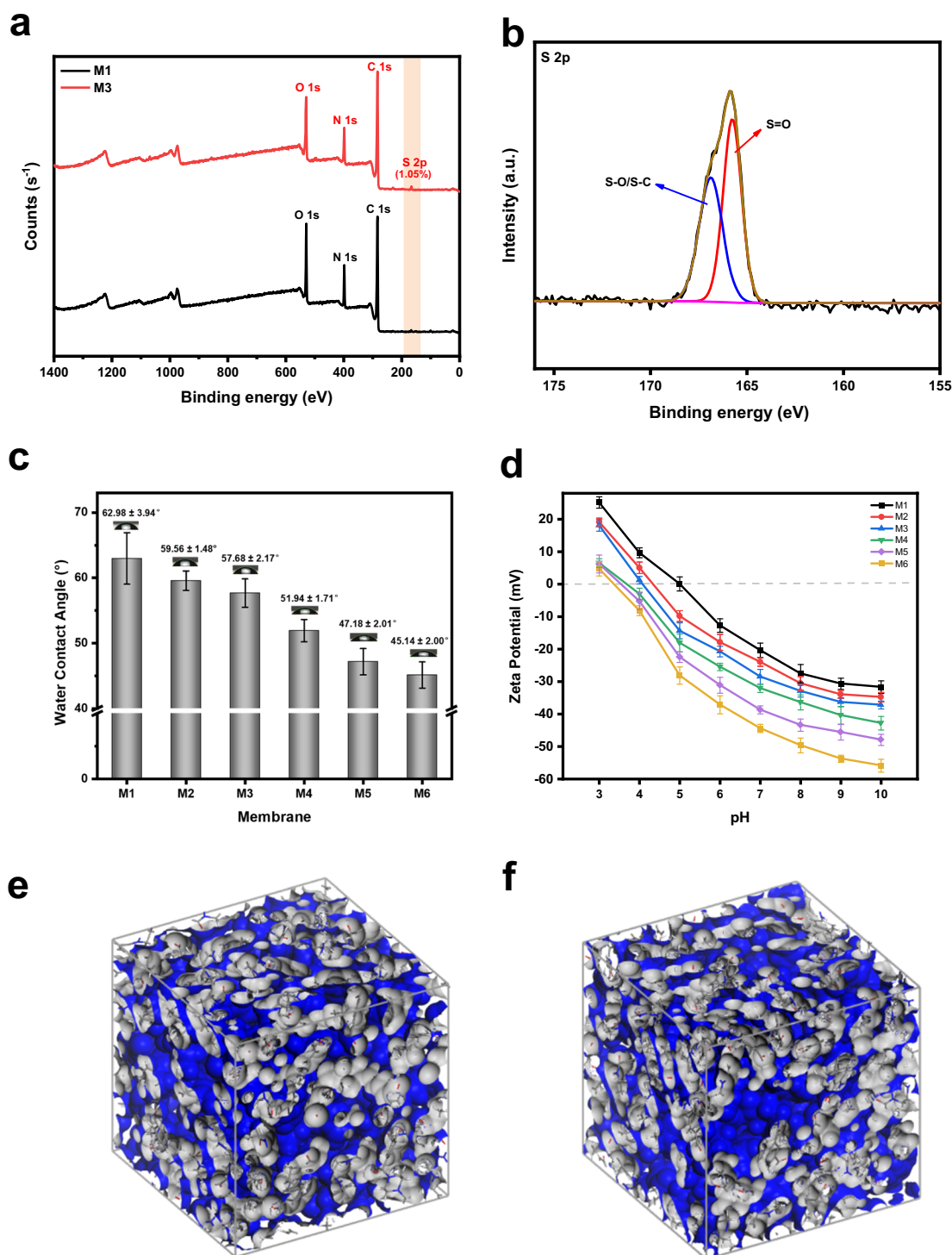
Fig. 5 | Membrane characterization. a The full-scan XPS spectra of M1 and M3, **b** the deconvoluted S 2p XPS spectrum of M3, **c** the WCA of M1–M6, **d** the Zeta potential of M1–M6, **e** and **f** the membrane free volume of M1 and M3 (acquired by MD simulation). The error bars represent the standard deviations of the data.

in the PA layer, which also contributes to the roughness of the membrane surface.

To obtain information about the functional groups on the membrane surface and to determine the effect of S-CONs on the degree of network crosslinking (DNC) of the PA layer, the spectra of C1s, N1s, and O1s on the surfaces of the TFC (M1) and TFN (M3) membranes were split-peak fitted, and the results are shown in Table 1 and Supplementary Fig. 7. Compared with M1, the DNC of the PA layer gradually increased with the addition of S-CONs. The increased DNC may be due to the fact that the added S-CONs

react with TMC to form an amide bond (–N–C=O)[44]. This would contribute to improving the membrane selectivity[45,46].

The water contact angle (WCA) of the membranes was used to measure the membrane hydrophilicity (Fig. 5c). At the amount of S-CONs added was 0.009 g, the WCA decreased from $62.98 \pm 3.94°$ (TFC) to $45.14 \pm 2.00°$ (M6), which means the membrane surface became more hydrophilic. This improvement was attributed to the S-CONs loaded with abundant hydrophilic sulfonic acid groups(–SO$_3$H), hydroxide (–OH), and ammonium (–NH$_2$) on the TFN-NF membrane surface. Besides, the zeta-

Table 1 | Relative content of surface functional groups of different membranes

No.	C1s			N1s			O1s	
	C–H /C–C /C=C (%)	C–N (%)	N–C=O/O–C=O (%)	R–NH$_2$ (%)	N–C=O (%)	R–N$^+$H$_3$ (%)	N–C=O (%)	O–C=O (%)
M1	54.77	31.84	13.34	25.04	66.44	8.52	53.54	46.46
M2	53.44	34.76	11.80	27.27	66.52	6.20	58.60	41.40
M3	52.30	35.58	12.12	11.88	67.48	20.64	63.23	36.77
M4	51.38	36.71	11.91	16.17	68.79	15.05	66.29	33.71
M5	50.50	36.94	12.56	12.56	68.95	18.49	72.81	15.99
M6	49.95	37.22	12.83	19.49	69.21	11.29	73.69	26.31

potential test results in Fig. 5d (Supplementary Table 1) indicated that the abundance of charging groups on the S-CONs also enhances the membrane electronegativity. At pH = 7.00, the electronegativity of the M3 membrane was -28.50 ± 2.27 mV, M6 was -44.41 ± 1.26 mV, while M1 was only -20.37 ± 2.22 mV. It is well known that the Donnan effect caused by the electronegativity is a key factor for anion rejection, therefore, the enhancement in electronegativity of the TFN membranes would help to improve the salt rejection. In addition, the free volume of the membrane affects the water permeance. Using the "Atom Volume & Surface" module of the MD simulation, a Connolly surface was constructed with a spherical probe (the radius of the probe was set to 0 Å)[47]. The free volumes of M1 and M3 were measured to be 38.07% and 39.08%, respectively. The higher free volumes of M3 could be more favorable for higher water permeance.

Separation performance of S-CONs NF membrane
Nanofiltration performance of S-CONs NF membrane. The separation performance of NF membranes is mainly reflected in two aspects: pure water permeance (PWP) and salt rejection. To determine the optimum loading concentrations of S-CONs, a series of TFN membranes were prepared by varying the concentration of S-CONs in the organic phase from 0.004 to 0.0100 g per 100 ml n-hexane, respectively. As shown in Fig. 6a, with the addition of S-CONs, the pure water permeance gradually increased and reached a maximum (8.84 L m^{-2} h^{-1} bar^{-1}) at an addition of 0.006 g, which was 1.75-folds larger than TFC (also named as M1, the membranes prepared without S-CONs, 5.07 L m^{-2} h^{-1} bar^{-1}) prepared under the same conditions. This could be attributed to the reduced PA layer thickness (Fig. 4a, b), improved roughness (Supplementary Table 1), and increased hydrophilicity (Fig. 5c). More importantly, the intrinsic pore of S-CONs, the pore formed between the S-CONs and the polyamide, and the pore formed by incomplete crosslinking simultaneously provide nanochannels for speedy transmission of water molecules and enhance the water permeance. However, the pure water permeance tended to decrease as the addition continued to increase. It is possible that the decrease of pure water permeance was caused by two simultaneous causes: one is that the increase in DNC makes the PA layer denser, and the water channels are reduced. The second is that the aggregation of S-CONs blocks the nanochannels[8,48]. The trend of permeance first grows and then declines with increasing S-CONs addition also applies to the salt solutions (Fig. 6b). In Fig. 6c, the inorganic salt rejection of the membranes followed the classical sequence in the literature: Na$_2$SO$_4$>MgSO$_4$>MgCl$_2$>NaCl[8,38]. It appeared that the salt rejection increases at first and then declines as the S-CONs addition amount increases. We attribute this to the fact that the increased DNC reduces the membrane pore size, which favors the size exclusion effect. And the abundance of sulfonic acid groups (–SO$_3$H), hydroxide (–OH), and ammonium (–NH$_2$) on the S-CONs enhances the Donnan effect of the membrane[49]. Figure 6d illustrates a schematic of water flow and ion separation of the TFN-NF membranes. Figure 6e was the water density along the z-axis (perpendicular to the membrane) for membranes with and without S-CONs calculated by MD simulations. This calculation provides a theoretical basis for the superior water permeance of TFN membranes[50]. The PEG test results in Fig. 6f demonstrated that the

effective pore diameter (μ_P) of TFN was only 0.36 nm, which was smaller than the pristine TFC membrane (0.38 nm).

The pressure resistance of the membranes was characterized by testing the membrane flux at different operating pressures (1.0–5.0 bar, step by 0.5 bar). First, the water flux corresponding to different operation pressures was obtained experimentally to get the data points in Fig. 6g. Then, the data points were fitted linearly to obtain the simulation results of R^2, which represented the linear relationship between the operation pressure and pure water flux. The better linear relationship of M3 indicated that the addition of S-CONs resulted in a higher compaction resistance of the TFN membrane[29,38]. By comparing the experimental data of other nanomaterials embedded as nanofillers in the PA layer in Fig. 6h (detailed information was given in Supplementary Table 2), it can be concluded that both the inherent pore structure and the abundant charge groups of S-CONs help to enhance the membrane permeance and Na$_2$SO$_4$ rejection.

Anti-fouling performance and stability of S-CONs NF membrane. The membrane anti-fouling performance was directly affected by surface hydrophilicity and electronegativity. In order to display the effect of S-CONs addition on membrane anti-fouling performance more intuitively, pure water (pH = 7.00) and BSA solution (1000 ppm, pH = 6.00) were used as the feed solution in turn for testing. As can be seen in Fig. 7a, the normalized flux of M1 and M3 declined to 0.80 and 0.96, respectively, at the end of the first "BSA contamination–pure water wash" cycle. After three "BSA–pure water" filtration cycles, the normalized flux of M1 decreased to 0.68, while M3 decreased only to 0.91, which exhibits promising anti-fouling performance. The improved anti-fouling performance was facilitated by the superior electronegativity and hydrophilicity of the M3. The enhanced electronegativity facilitates electrostatic repulsion between the membrane surface and the BSA. The strong electronegativity enhances the electrostatic repulsion between the membrane and the BSA, as both are negatively charged. In addition, the enhanced hydrophilicity means that the ability of the hydrated layer to adsorb contaminants is also enhanced, resulting in superior anti-fouling performance of the TFN membrane.

Long-lasting operational stability of M1 and M3 was tested for 51 days using Na$_2$SO$_4$ (2000 ppm) as feed solution (Fig. 7b). The pristine TFC membrane (M1) permeate flux and Na$_2$SO$_4$ rejection decreased by 27.70% and 2.60%, respectively, while M3 decreased by only 13.90% and 0.94%. The superior long-term operation stability of M3 also demonstrated that the S-CONs can be stably fixed on PA layers, which was attributed to the covalent bond formed between the PA layer and S-CONs (Fig. 2d, e). The intrinsic pore size of the nanosheets provides a stable nano-channel for water permeation, while the charge loaded by the nanosheets provides stable electrostatic repulsion and maintains a high Na$_2$SO$_4$ rejection.

Chlorine resistance of S-CONs NF membrane. Whether in use or in the cleaning process, NF membranes were inevitably exposed to hypochlorite disinfectants, and the cross-linked network formed by the chemical bonding and internal hydrogen bonding of the PA layer can be destroyed by chlorine oxidation (Supplementary Fig. 8)[51]. Therefore, the chlorine resistance of membranes is also an important factor in

Fig. 6 | Membrane performance. a The pure water permeance and Na_2SO_4 rejection, **b** the permeance of salt solution, **c** the salt rejection, **d** the schematic of the water flow and ion separation, **e** the water density along the *z*-axis (perpendicular to the membrane) for membranes with and without S-CONs (acquired by MD simulation), **f** the MWCO of M1 and M3, **g** the pressure resistance of M1 and M3, **h** comparison of separation performance of M3 with other NF membranes. The error bars represent the standard deviations of the data.
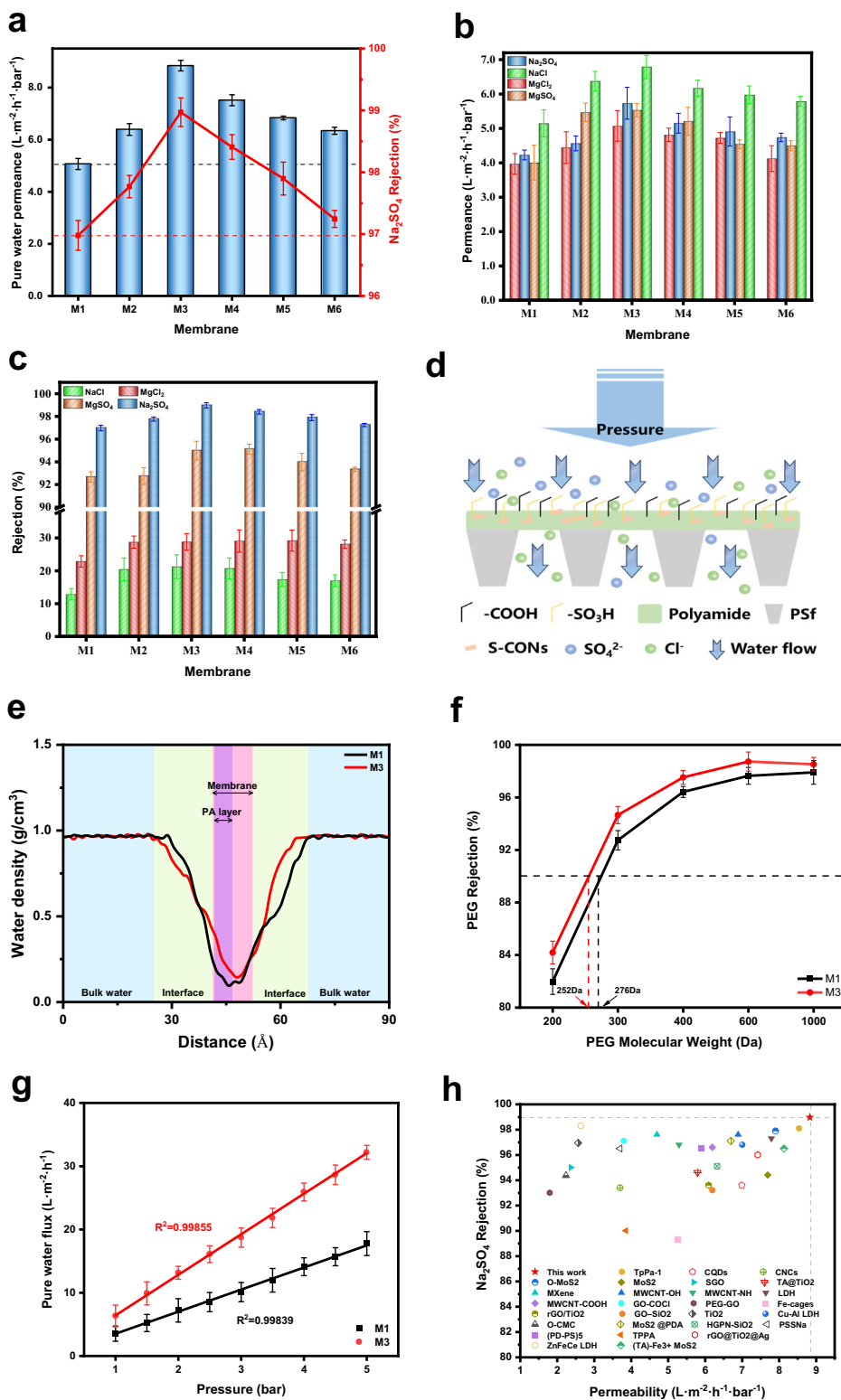
quantifying the durability of membranes. Ettori et al.[52] found that the N-chlorination of amide bonds and the accompanying Orton rearrangement cyclic chlorination[53] could break the chemical bonds in the membranes and disrupt the integrity of the membrane structure, which in turn decreased the separation performance of the membranes.

In this section, we explored the chlorine resistance of M1, M3, and M6 at different pH (pH = 5.00 and 10.00) and chlorine exposure intensities. The results (Fig. 8) indicated that the addition of S-CONs facilitates

the improvement of the membrane chlorine resistance, and the higher the addition amounts of S-CONs, the smaller the decrease in water permeance and Na_2SO_4 rejection. There are several reasons for the improved chlorine resistance of TFN membranes. (1) The S-CONs featured rich secondary amide groups might covalently manipulate the PA layer by the formation of tertiary amide groups (Figs. 8c and 2d, e), which are less susceptible to chlorine attack due to the lack of –N–H amide groups[54]. (2) The functional groups of S-CONs could enhance the intermolecular hydrogen bonding
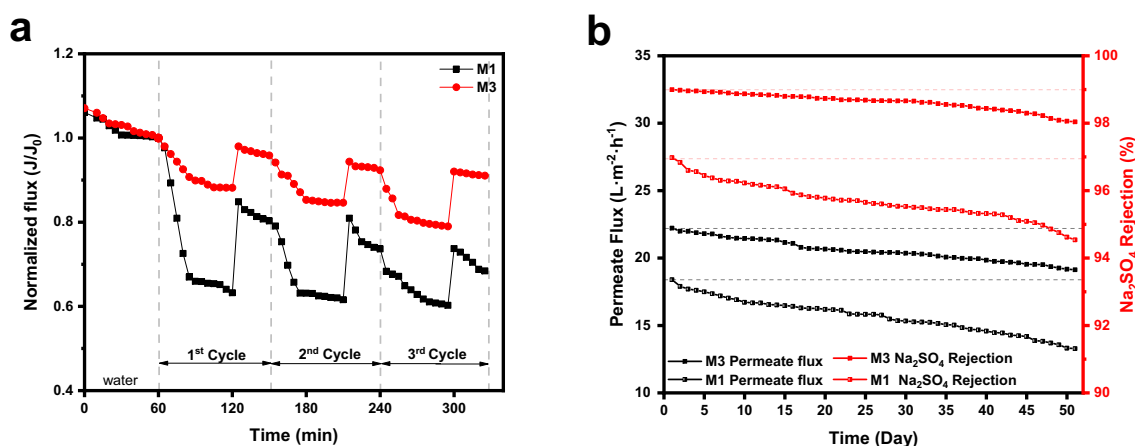
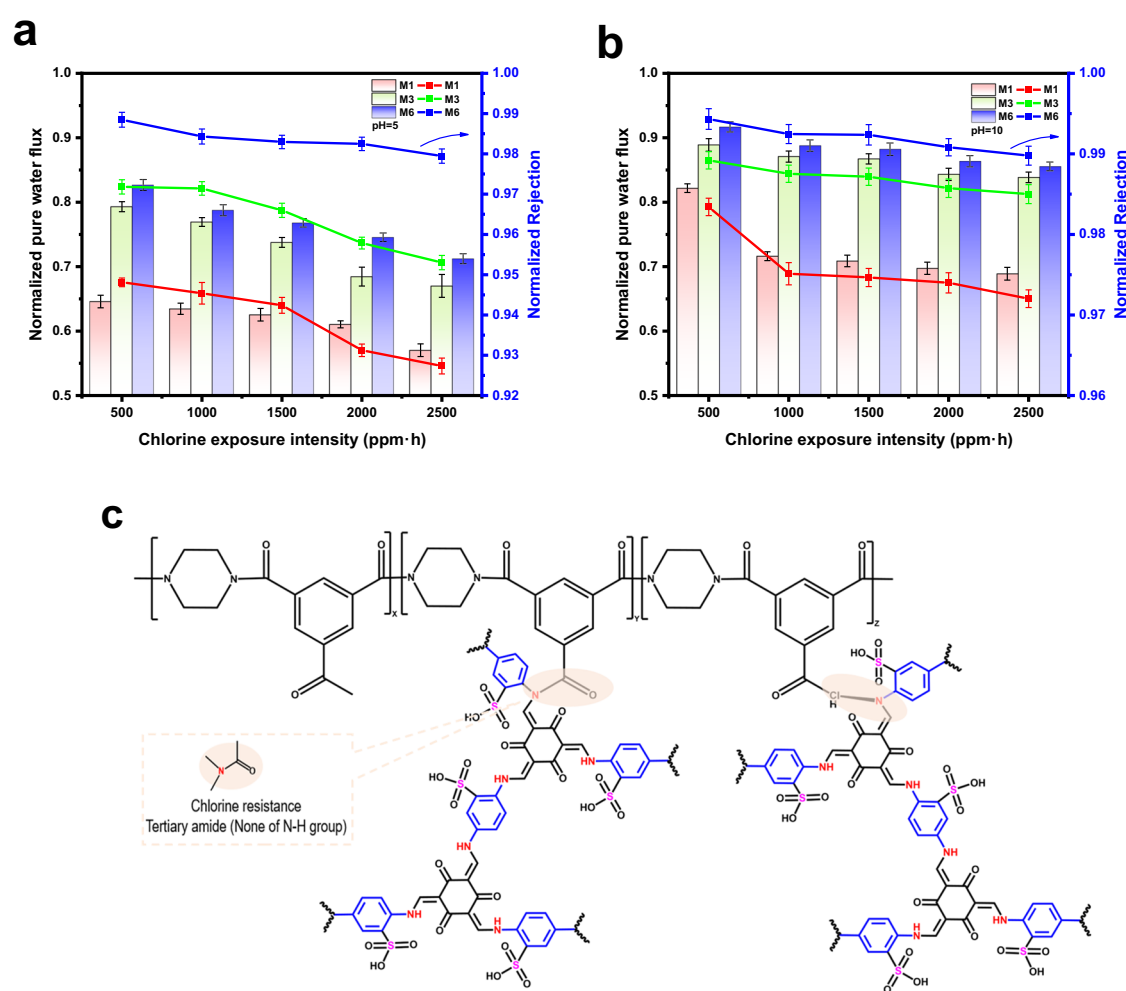**Fig. 7 | Membrane performance. a** The anti-fouling performance of M1 and M3 and **b** the stability of M1 and M3.

Fig. 8 | Membrane chlorine resistance. a Normalized pure water flux and normalized Na_2SO_4 rejection at pH = 5, **b** normalized pure water flux and normalized Na_2SO_4 rejection at pH = 10, and **c** the reaction between S-CONs and polyamide chains. The error bars represent the standard deviations of the data.

effect. Thus, the TFN-NF membranes had better chlorine resistance than the TFC-NF membrane[55,56]. (3) The high electronegativity of M3 and M6 could effectively prevent the contact between active chlorine and the membrane surface by more powerful electrostatic repulsion and thus prevent the active chlorine from disrupting the polyamide layer[57,58]. Moreover, separation performance decreased significantly more at pH = 5.00 than at pH = 10.00. This was attributed to the fact that active chlorine is more easily converted to HOCl under acidic conditions[54,59], which damages the membrane structure more severely[60,61].

In summary, this study successfully incorporated sulfonated covalent organic framework nanosheets (S-CONs) as nanofillers into the PA layer to modify the TFC membrane. The results showed that the charged groups (such as $-SO_3H$, $-NH_2$, and $-OH$) loaded on S-CONs can effectively improve the hydrophilicity and electronegativity of the TFN membranes.

The pure water permeance reached $8.84 \, \text{L} \, \text{m}^{-2} \, \text{h}^{-1} \, \text{bar}^{-1}$ (about 1.75 times that of the TFC membrane), and the Na_2SO_4 rejection improved to 98.97% when the S-CONs added amount was 0.006 g. More interestingly, the chlorine resistance of the membranes was improved due to the formation of amide bonds between S-CONs and TMC. This study reveals the potential of using 2D functionalized COFs as nanofillers to modify TFC membranes for efficient nanofiltration.

Methods
Materials
The pure water permeance and BSA rejection of lab-made supporting substrates PSf-UF membrane was about $300.00 \, \text{L} \, \text{m}^{-2} \, \text{h}^{-1} \, \text{bar}^{-1}$ and 99.00%, respectively. 2,4,6-Triformylphloroglucinol (Tp, ≥97%, Macklin) and 1,4-Phenylenediamine-2-sulfonic acid (Pa-SO_3H, ≥99%, Macklin) were used to synthesis Tp Pa-SO_3H COFs (S-COFs). 1,4-Dizacyclohexane (PIP, 99%, Macklin) and 1,3,5-Trichlorobenzoylchloride (TMC, 98%, Macklin) were used for interfacial polymerization (IP) reaction to prepare PA layers. In addition to PIP, DL-10-Camphorsulfonic acid (CSA, 99%, Macklin), N, N-diethylethanamine (TEA, 99%, Macklin) and dodecyl-sulfonic-acid sodium (SDS, 99%, Macklin) are added as additives to the aqueous phase, while TMC was dissolved in n-hexane (97%, Macklin) as the organic phase.

The separation performance was examined with four inorganic salts: Na_2SO_4 (99%), $MgSO_4$ (98%), NaCl (99.5%), and $MgCl_2$ (99.5%), which were all purchased from Sinopharm. The molecular weight cut-off (MWCO) was measured by a nanofiltration experiment with PEG (Poly (ethylene glycol)) of different molecular weights at 200, 300, 400, 600, and 1000 Da, purchased from Aladdin Reagent Company. All reagents are used according to the purchase specifications and no further follow-up was carried out.

Preparation of S-CONs
In this study, the S-COFs were synthesized by the solvothermal synthesis method. More specifically, Pa-SO_3H and Tp were dissolved in a certain amount of ethanol by ultrasonic dispersion. The homogenized solution was packed into a PTFE reactor, and then the autoclave was filled with nitrogen and sealed off. The S-COFs were obtained after heating 72 h at 120 °C. Prior to characterization and further experiments, the red-brown powder was washed with N, N-dimethylformamide (DMF), and ethanol sequentially. The pure sample free of unreacted monomers was obtained by vacuum-drying (12 h, 60 °C).

According to our previous studies it has been demonstrated that the mechanical grinding method would not change the crystal structure and chemical structure of the COFs[22]. Therefore, we still exfoliated S-COFs with a mechanical grinding method to obtain S-CONs[62]. In particular, 50 mg S-COFs and 1–2 drops of methanol were added to a mortar (i.d. = 75.00 mm). After grounding continuously for 0.5 h, the powder was dispersed in about 0.1 L methanol, centrifuged at 7000 rpm/min for 10 min, and dried at 50 °C for 12 h to acquire S-CONs powders for the next step.

Characterization of S-CONs
The micro-morphology of S-CONs was observed by FE-SEM (S-4800, HITACHI, Japan, 5 kV, 10 μA) and TEM (Talos-S, FEI, USA, 100 kV, 20 μA); the elemental composition and chemical structure were characterized by EDX (Oxford 6587, HITACHI, Japan, attached to the FE-SEM) and ATR-FTIR (iS10, Thermo, USA) spectroscopy as well as XPS (Thermo Escalab 250 Xi, USA); the crystal structure of the nanosheets was tested by P-XRD (X'Pert Pro, PANalytical, The Netherlands, 40 kV, 40 mA); the thickness was tested by AFM (Dimension 3100, Bruker, USA); the zeta-potential at pH = 2–10 in water and particle lateral size distribution in n-hexane were measured by ZetaPALS (Zetasizer Nano S90, Malvern Panalytical, UK).

Preparation of S-CONs NF membrane
Before the experiments, the lab-made PSf substrates were soaked in distilled (DI) water for 12 h, and freshwater was substituted every 3 h to remove

Table 2 | The aqueous and organic phase solution preparation scheme

Aqueous phase solution	DI water (wt%)	CSA (wt%)	TEA (wt%)	PIP (wt%)	SDS (wt%)
	95.95	1.50	1.50	1.00	0.05
Organic phase solution	n-hexane (wt%)	TMC (wt%)	SA-CONs (g/100 ml)		
	99.85	0.15	0-0.0100		

$NaSO_3$H from the membrane surface. It was added to keep the freshness of the substrate. Then the PSf substrates were glued on the epoxy frame with double-sided adhesive, and the water droplets on the surface of the substrates were removed with a soft paper towel meticulously[63]. Simultaneously, the aqueous phase (distilled water as solvent) and organic phase (n-hexane as solvent) solutions were formulated according to Table 2. Then the TFC/TFN-NF membranes were prepared by the conventional IP reaction in the laboratory. Firstly, a 50 ml aqueous phase was poured into the epoxy frame for 80 s to obtain a substrate impregnated with PIP. Then, the surplus aqueous solution was poured out, and the substrate was dried at room temperature. Thirdly, 50 ml organic phase solution was poured into the epoxy frame and removed after 5 s. Finally, the membranes were heat-treated at 50 °C for 1 min to enhance the cross-linking. The obtained NF membranes were socked in distilled water at 4 °C for subsequent experiments.

The experiments were conducted at room temperature (25.00 ± 3.00 °C) with humidity of 60.00–70.00%. To ensure reproducibility, each identical recipe was carried out at least 10 times, and each time, at least five membrane samples were taken for performance testing.

The main steps in the preparation of S-CONs and TFN-NF membranes are shown in Fig. 9a.

S-CONs were added in units of n-hexane per 100 ml, and the addition amounts of M1–M6 were 0.000, 0.004, 0.006, 0.007, 0.009, and 0.0100 g, respectively.

Characterization of S-CONs NF membrane
The surface and cross-sectional micro-morphology of the membranes were investigated by FE-SEM (S-4800, HITACHI, Japan, 5 kV, 10 μA). The samples for cross-sectional detection were obtained by rupturing the nonwoven-free PSf layer in liquid nitrogen. All the membrane samples were sputtered with Pt by a Q150T turbo-pumped sputter coater with a current of 25 mA for 120 s before SEM characterization.

The thickness of the PA layer was evaluated by TEM (Talos-S, FEI, USA, 100 kV, 20 μA). The membrane samples were embedded in epoxy resin and then cut into slices (about 100 nm in thickness) by an ultra-microtome (Leica Ultracut R). Then, the slice-shaped samples were fixed on the carbon-coated copper grid.

AFM (Dimension 3100, Bruker, USA) was conducted to analyze the membranes roughness with 5 μm × 5 μm; XPS (Thermo Escalab 250 Xi, USA), P-XRD (X'Pert Pro, PANalytical, The Netherlands, 40 kV, 40 mA) and EDX (Oxford 6587, HITACHI, Japan) were applied to check the surface elemental composition, measure the crystallinity of membrane surface.

The degree of cross-linking (DNC) value of the PA layer according to Eq. (1):

$$\text{Degree of crosslinking}\,(\%) = \frac{C_{-CONH-}}{C_{-CONH-} + C_{-COO-}} \times 100 \qquad (1)$$

where C_{-CONH-} means the amide groups content and C_{-COO-} means the carboxyl groups content in the PA layer.

SurPASS 3 (Anton Paar, Australia), a streaming potential analyzer, was used to assess the zeta potential. The gap height was adjusted to about 100.00 ± 5.00 μm, 10 mM KCl was used as the background electrolyte
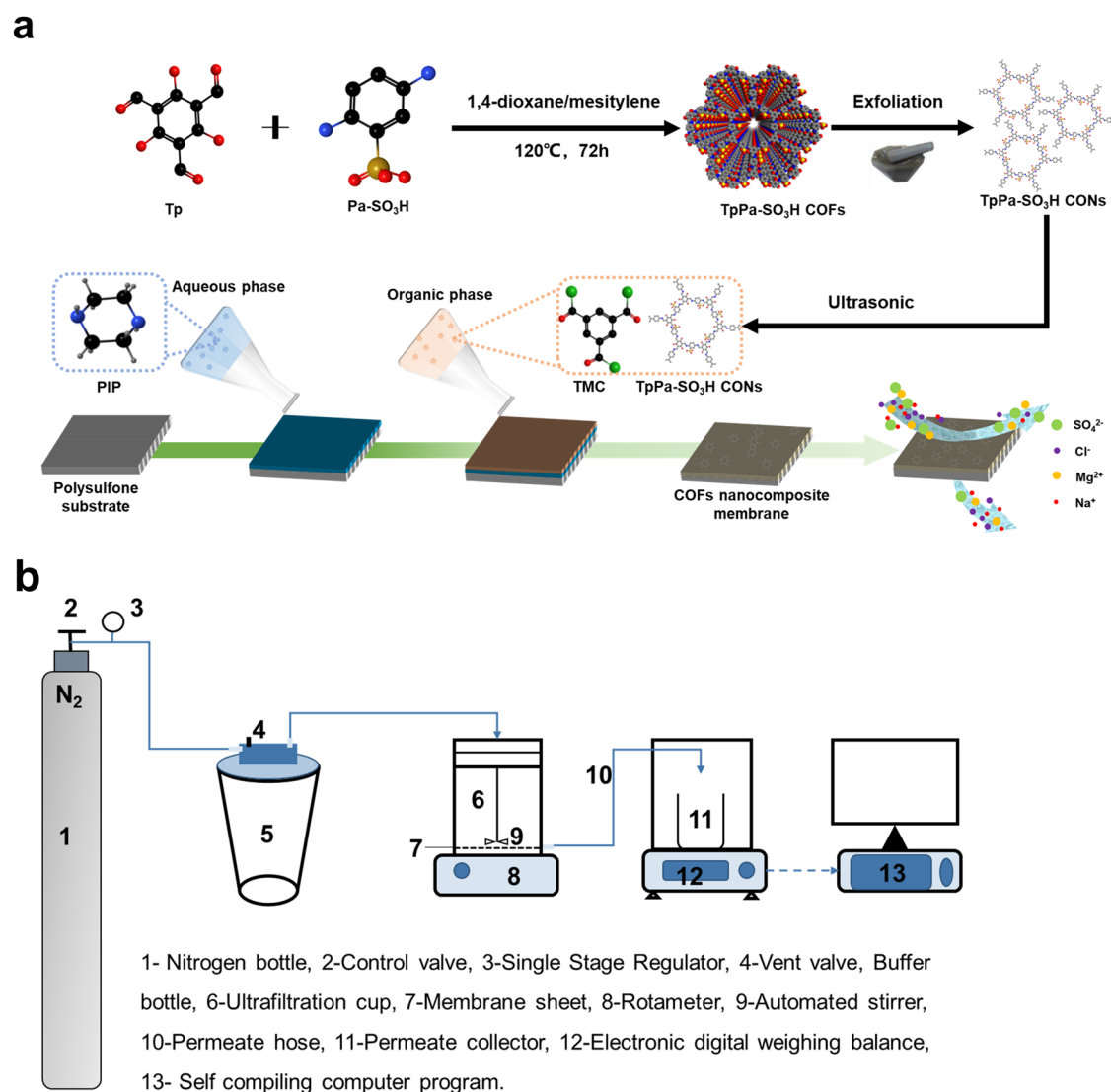
Fig. 9 | Synthesis scheme and testing apparatus. a The synthesis scheme of S-CONs and S-CONs nanocomposite membrane, **b** the lab-assembled dead-end testing apparatus.

solution, and 50 mM HCl and 50 mM NaOH were used as pH regulators, respectively[8,22,63].

DSA100 (KRUSS, German) was used for investigating the membrane hydrophilicity properties with DI water as the reference solvent, the water contact angle for each sample was repeated for at least ten random points, and the average data was reported.

Separation performance of S-CONs NF membrane

The characterize experiments were performed using the lab-assembled dead-end apparatus as shown in Fig. 9b. The characterization of membrane separation performance mainly included a nanofiltration experiment, pressure-flux test, anti-fouling performance test, long-lasting operation stability test, and chlorine resistance test. Except for the pressure-flux test, all tests were performed at an operating pressure of 4.0 bar. Each membrane was normalized by pre-compressed at least 30 and 10 min pre-filtration test, followed filtration test for 20 min to achieve a stable experimental state. The weight changes of the permeate solution were collected by the electronic balance and connected to a computer for storage. To ensure reproducibility, each identical recipe was carried out at least 10 times, and each time, at least five membrane samples were taken for testing, and the average value was calculated to obtain the results.

Nanofiltration experiment of S-CONs NF membrane

The nanofiltration experiment included a pure water permeance test and an inorganic salts (2000 ppm) rejection test.

The pure water permeance P_w ($L \cdot m^{-2} \cdot h^{-1} \cdot bar^{-1}$) was calculated by Eq. (2):

$$P_w = \frac{V}{A \cdot t \cdot \Delta P} \qquad (2)$$

in which V refers to the total permeate volume (L), t refers to the NF test time (h), and A is the actual permeate area of each membrane (m²), ΔP is the operation pressure (4 bar).

The rejection of each membrane was calculated by Eq. (3):

$$R = 1 - \frac{C_p}{C_f} \times 100\% \qquad (3)$$

in which C_p ($g \cdot L^{-1}$) and C_f ($g \cdot L^{-1}$) represent the permeate concentrations and feed concentrations, respectively. For the salt solution, the conductivity of the solution was measured with a conductivity meter to calculate the values of C_p and C_f.

For the PEG solution, the total organic carbon content (TOC) was measured to acquire the values of C_P and C_f. The pore diameter was calculated according to the Stokes radius formula shown in Eq. (4):

$$a = 16.73 \times 10^{-10} M^{0.557} \tag{4}$$

in which a (cm) means the Stokes radius and M means the PEG molecular weight.

The MD simulation of the water-solvated membrane system was performed in the NPT ensemble at 300 K and 1 atm. And a graphene sheet was used as a virtual piston to control the pressure.

Anti-fouling performance and stability test of S-CONs NF membrane

Anti-fouling performance tests were carried out with pure water and BSA (1000 ppm) solution alternately as feed solution. We define the stable flux obtained after the first 30 min pure water nanofiltration as the initial flux (J_0), the flux at moment t is recorded as J_0. The flux recovery rate (FRR) was calculated to assess the membrane anti-fouling performance by Eq. (5):

$$\text{FRR} = \frac{J}{J_0} \times 100\% \tag{5}$$

in which J was the tested permeate and J_0 was the stable permeate. J and J_0 were calculated by Eq. (6)

$$J = \frac{V}{A \cdot t} \tag{6}$$

A long-lasting operation stability test was carried out with 2000 ppm Na_2SO_4 at 4 bar pressure for 51-day nanofiltration, the salt solution permeance and Na_2SO_4 rejection were calculated using Eqs. (6) and (3).

Chlorine resistance test of S-CONs NF membrane

The chlorine resistance of the membrane was tested by static accelerating chlorination experiments. M1, M3, and M6 were immersed in 500 ppm NaClO solution under dark conditions for 5 h discontinuity at pH = 5.00 and pH = 10.00, which was regulated with 100 mM HCl or 100 mM NaOH, respectively. At one-hour intervals, the membranes were washed and soaked in pure water for 24 h. Then the membranes were subjected to nanofiltration experiments with pure water and 2000 ppm Na_2SO_4 solution under 4.0 bar to test the membrane performance. The degree of chlorination was represented by the total exposure to free chlorine amount (ppm·h). Normalized pure water flux and normalized Na_2SO_4 rejection were calculated by Eqs. (7) and (8) to better investigate the influence of chlorination on the membrane.

$$\text{Normalized pure water flux} = \frac{J_x}{J_0} \times 100\% \tag{7}$$

$$\text{Normalized } Na_2SO_4 \text{ rejection} = \frac{R_x}{R_0} \times 100\% \tag{8}$$

in which J_x and R_x were the pure water flux and the Na_2SO_4 rejection after x ($x = 1$–5) h of chlorine exposure, respectively. J_0 and R_0 were the pure water flux and the Na_2SO_4 rejection before chlorination experiments. The calculation of J and R were given in Eqs. (6) and (3).

Data availability

All data generated or analyzed during this study are included in this published article (and its supplementary information files).

References

1. Lu, X., Boo, C., Ma, J. & Elimelech, M. Bidirectional diffusion of ammonium and sodium cations in forward osmosis: role of membrane active layer surface chemistry and charge. *Environ. Sci. Technol.* **48**, 14369–14376 (2014).
2. Liang, Y. et al. Polyamide nanofiltration membrane with highly uniform sub-nanometre pores for sub-1 Å precision separation. *Nat. Commun.* **11**, 2015 (2020).
3. Yang, C. et al. Ultrathin nanofiltration membrane assembled by polyethyleneimine-grafted graphene quantum dots. *J. Membr. Sci.* **642**, 119944 (2022).
4. Sarkar, P., Modak, S. & Karan, S. Ultraselective and highly permeable polyamide nanofilms for ionic and molecular nanofiltration. *Adv. Funct. Mater.* **31**, 2007054 (2020).
5. Geise, G. M., Park, H. B., Sagle, A. C., Freeman, B. D. & McGrath, J. E. Water permeability and water/salt selectivity tradeoff in polymers for desalination. *J. Membr. Sci.* **369**, 130–138 (2011).
6. Jeong, B.-H. et al. Interfacial polymerization of thin film nanocomposites: a new concept for reverse osmosis membranes. *J. Membr. Sci.* **294**, 1–7 (2007).
7. Hu, R., Zhang, R., He, Y., Zhao, G. & Zhu, H. Graphene oxide-in-polymer nanofiltration membranes with enhanced permeability by interfacial polymerization. *J. Membr. Sci.* **564**, 813–819 (2018).
8. Yang, S., Jiang, Q. & Zhang, K. Few-layers 2D O-MoS$_2$ TFN nanofiltration membranes for future desalination. *J. Membr. Sci.* **604**, 118052 (2020).
9. Sun, H. & Wu, P. Tuning the functional groups of carbon quantum dots in thin film nanocomposite membranes for nanofiltration. *J. Membr. Sci.* **564**, 394–403 (2018).
10. Lau, W. J. et al. A review on polyamide thin film nanocomposite (TFN) membranes: history, applications, challenges and approaches. *Water Res* **80**, 306–324 (2015).
11. Xue, S.-M., Ji, C.-H., Xu, Z.-L., Tang, Y.-J. & Li, R.-H. Chlorine resistant TFN nanofiltration membrane incorporated with octadecylamine-grafted GO and fluorine-containing monomer. *J. Membr. Sci.* **545**, 185–195 (2018).
12. Chen, Y. et al. Enhancing the NaCl/Na$_2$SO$_4$ separation selectivity and chlorine resistance of nanofiltration membranes by incorporating novel designed starch nanoparticles. *Appl. Surf. Sci.* **604**, 154417 (2022).
13. Wu, X., Fang, F., Zhang, B., Wu, J. J. & Zhang, K. Biogenic silver nanoparticles-modified forward osmosis membranes with mitigated internal concentration polarization and enhanced antibacterial properties. *npj Clean Water* **5**, 50 (2022).
14. Zhao, H. et al. Improving the performance of polyamide reverse osmosis membrane by incorporation of modified multi-walled carbon nanotubes. *J. Membr. Sci.* **450**, 249–256 (2014).
15. Liu, S. et al. High performance internally pressurized hollow fiber thin-film nanocomposite nanofiltration membrane incorporated with tannic acid functionalized MoS$_2$ nanosheets for wastewater treatment. *Desalination* **547**, 116227 (2023).
16. Liao, Z., Zhu, J., Li, X. & Van der Bruggen, B. Regulating composition and structure of nanofillers in thin film nanocomposite (TFN) membranes for enhanced separation performance: a critical review. *Sep. Purif. Technol.* **266**, 118567 (2021).
17. Xu, H. et al. Covalent organic frameworks-incorporated thin film composite membranes prepared by interfacial polymerization for efficient CO$_2$ separation. *Chin. J. Chem. Eng.* **43**, 152–160 (2022).
18. Yang, C. X., Liu, C., Cao, Y. M. & Yan, X. P. Facile room-temperature solution-phase synthesis of a spherical covalent organic framework for high-resolution chromatographic separation. *Chem. Commun.* **51**, 12254–12257 (2015).
19. Li, C. et al. Covalent organic frameworks (COFs)-incorporated thin film nanocomposite (TFN) membranes for high-flux organic solvent nanofiltration (OSN). *J. Membr. Sci.* **572**, 520–531 (2019).

20. Wang, C. et al. Covalent organic framework modified polyamide nanofiltration membrane with enhanced performance for desalination. *J. Membr. Sci.* **523**, 273–281 (2017).

21. Khan, N. A. et al. Incorporating covalent organic framework nanosheets into polyamide membranes for efficient desalination. *Sep. Purif. Technol.* **274**, 119046 (2021).

22. Meng, W., Zhu, J., Xue, Q. & Zhang, K. Incorporating imine-based covalent organic frameworks nanosheet as an active filler for long-term nanofiltration desalination. *J. Membr. Sci.* **683**, 121712 (2023).

23. Xu, L., Yang, T., Li, M., Chang, J. & Xu, J. Thin-film nanocomposite membrane doped with carboxylated covalent organic frameworks for efficient forward osmosis desalination. *J. Membr. Sci.* **610**, 118111 (2020).

24. Jiang, Y. et al. Two dimensional COFs as ultra-thin interlayer to build TFN hollow fiber nanofiltration membrane for desalination and heavy metal wastewater treatment. *J. Membr. Sci.* **635**, 119523 (2021).

25. Barry, E., McBride, S. P., Jaeger, H. M. & Lin, X.-M. Ion transport controlled by nanoparticle-functionalized membranes. *Nat. Commun.* **5**, 5847 (2014).

26. Yadav, V., Rajput, A. & Kulshrestha, V. Sulfonated Poly(ether sulfone) based sulfonated molybdenum sulfide composite membranes and their applications in salt removal and alkali recovery. *J. Membr. Sci.* **603**, 118043 (2020).

27. Yang, W. et al. A polyamide membrane with tubular crumples incorporating carboxylated single-walled carbon nanotubes for high water flux. *Desalination* **479**, 114330 (2020).

28. Kang, Y., Obaid, M., Jang, J. & Kim, I. S. Sulfonated graphene oxide incorporated thin film nanocomposite nanofiltration membrane to enhance permeation and antifouling properties. *Desalination* **470**, 114125 (2019).

29. Zhu, J., Meng, W., Xue, Q. & Zhang, K. Two dimensional sulfonated molybdenum disulfide (S-MoS$_2$) thin-film nanocomposite nanofiltration membrane for selective desalination. *J. Membr. Sci.* **676**, 121574 (2023).

30. Yuan, S. et al. Covalent organic frameworks for membrane separation. *Chem. Soc. Rev.* **48**, 2665–2681 (2019).

31. Xue, S. M., Xu, Z. L., Tang, Y. J. & Ji, C. H. Polypiperazine-amide nanofiltration membrane modified by different functionalized multiwalled carbon nanotubes (MWCNTs). *ACS Appl. Mater. Interfaces* **8**, 19135–19144 (2016).

32. He, Y., Zhao, D. L. & Chung, T.-S. Na+ functionalized carbon quantum dot incorporated thin-film nanocomposite membranes for selenium and arsenic removal. *J. Membr. Sci.* **564**, 483–491 (2018).

33. Wang, X. et al. Construction of thin-film nanocomposite membranes by incorporating acyl chloride@MoS$_2$ for enhanced nanofiltration performance. *Sep. Purif. Technol.* **319**, 124078 (2023).

34. Wen, P. et al. Polyamide thin film composite nanofiltration membrane modified with acyl chlorided graphene oxide. *J. Membr. Sci.* **535**, 208–220 (2017).

35. Dai, R. et al. Hydrophilic selective nanochannels created by metal organic frameworks in nanofiltration membranes enhance rejection of hydrophobic endocrine-disrupting compounds. *Environ. Sci. Technol.* **53**, 13776–13783 (2019).

36. Wang, M. et al. Constructing channel-mediated facilitated transport membranes by incorporating covalent organic framework nanosheets with tunable microenvironments. *J. Mater. Chem. A* **7**, 9912–9923 (2019).

37. Tayel, A., Abdelaal, A. B., Esawi, A. M. K. & Ramadan, A. R. Thin-film nanocomposite (TFN) membranes for water treatment applications: characterization and performance. *Membranes* **13**, 477 (2023).

38. Xue, Q. & Zhang, K. MXene nanocomposite nanofiltration membrane for low carbon and long-lasting desalination. *J. Membr. Sci.* **640**, 119808 (2021).

39. Tan, Z., Chen, S., Peng, X., Zhang, L. & Gao, C. Polyamide membranes with nanoscale Turing structures for water purification. *Science* **360**, 518–521 (2018).

40. Gu, Z. et al. Incorporation of lysine-modified UiO-66 for the construction of thin-film nanocomposite nanofiltration membrane with enhanced water flux and salt selectivity. *Desalination* **493**, 114661 (2020).

41. Song, N. et al. Tailoring nanofiltration membrane with three-dimensional turing flower protuberances for water purification. *J. Membr. Sci.* **621**, 118985 (2021).

42. Cheng, D. et al. Incorporating of β-cyclodextrin based nanosheet for advanced thin-film nanocomposite nanofiltration membrane with improved separation and anti-fouling performances. *J. Membr. Sci.* **685**, 121969 (2023).

43. He, Y. et al. Improving the anti-fouling property and permeate flux of hollow fiber composite nanofiltration membrane using β-cyclodextrin. *Sci. Rep.* **9**, 12435 (2019).

44. Yang, C. et al. Effectively regulating interfacial polymerization process via in-situ constructed 2D COFs interlayer for fabricating organic solvent nanofiltration membranes. *J. Membr. Sci.* **637**, 119618 (2021).

45. Zhang, N., Song, X., Jiang, H. & Tang, C. Y. Advanced thin-film nanocomposite membranes embedded with organic-based nanomaterials for water and organic solvent purification: A review. *Sep. Purif. Technol.* **269**, 118719 (2021).

46. Abdikheibari, S., Lei, W., Dumée, L. F., Barlow, A. J. & Baskaran, K. Novel thin film nanocomposite membranes decorated with few-layered boron nitride nanosheets for simultaneously enhanced water flux and organic fouling resistance. *Appl. Surf. Sci.* **488**, 565–577 (2019).

47. Cai, W., Wang, M., Yang, G. Q. & Li, J. High-performance nanofiltration membranes with a polyamide-polyester composite layer and a polydopamine surface layer for desalination and dye pollutant removal. *Polymer* **268**, 125720 (2023).

48. Yin, J., Zhu, G. & Deng, B. Graphene oxide (GO) enhanced polyamide (PA) thin-film nanocomposite (TFN) membrane for water purification. *Desalination* **379**, 93–101 (2016).

49. Zhao, Y. et al. Differentiating solutes with precise nanofiltration for next generation environmental separations: a review. *Environ. Sci. Technol.* **55**, 1359–1376 (2021).

50. Araki, T. et al. Molecular dynamics study of carbon nanotubes/polyamide reverse osmosis membranes: polymerization, structure, and hydration. *ACS Appl. Mater. Interfaces* **7**, 24566–24575 (2015).

51. Meng, Q. W. & Ge, Q. Enhancing chlorine resistance and water permeability during forward osmosis separation using superhydrophilic materials with conjugated systems. *ACS Appl. Mater. Interfaces* **12**, 35393–35402 (2020).

52. Ettori, A., Gaudichet-Maurin, E., Schrotter, J.-C., Aimar, P. & Causserand, C. Permeability and chemical analysis of aromatic polyamide based membranes exposed to sodium hypochlorite. *J. Membr. Sci.* **375**, 220–230 (2011).

53. Do, V. T., Tang, C. Y., Reinhard, M. & Leckie, J. O. Degradation of polyamide nanofiltration and reverse osmosis membranes by hypochlorite. *Environ. Sci. Technol.* **46**, 852–859 (2012).

54. Huang, H., Lin, S., Zhang, L. & Hou, L. Chlorine-resistant polyamide reverse osmosis membrane with monitorable and regenerative sacrificial layers. *ACS Appl. Mater. Interfaces* **9**, 10214–10223 (2017).

55. Liu, S. et al. Enhancement of desalination performance of thin-film nanocomposite membrane by cellulose nanofibers. *J. Membr. Sci.* **592**, 117363 (2019).

56. Liu, M., Chen, Z., Yu, S., Wu, D. & Gao, C. Thin-film composite polyamide reverse osmosis membranes with improved acid stability and chlorine resistance by coating N-isopropylacrylamide-co-acrylamide copolymers. *Desalination* **270**, 248–257 (2011).

57. Li, Y. et al. Graphene quantum dot engineered ultrathin loose polyamide nanofilms for high-performance nanofiltration. *J. Mater. Chem. A* **8**, 23930–23938 (2020).

58. Song, X., Zhou, Q., Zhang, T., Xu, H. & Wang, Z. Pressure-assisted preparation of graphene oxide quantum dot-incorporated reverse

osmosis membranes: antifouling and chlorine resistance potentials. *J. Mater. Chem. A* **4**, 16896–16905 (2016).

59. Xu, J., Wang, Z., Yu, L., Wang, J. & Wang, S. A novel reverse osmosis membrane with regenerable anti-biofouling and chlorine resistant properties. *J. Membr. Sci.* **435**, 80–91 (2013).
60. Kwon, Y.-N., Tang, C. Y. & Leckie, J. O. Change of membrane performance due to chlorination of crosslinked polyamide membranes. *J. Appl. Polym. Sci.* **102**, 5895–5902 (2006).
61. You, M. et al. Probing and relating the morphology, structure and performance evolution of low pressure RO membranes under chlorine exposure. *J. Environ. Chem. Eng.* **9**, 106223 (2021).
62. Chandra, S. et al. Chemically stable multilayered covalent organic nanosheets from covalent organic frameworks via mechanical delamination. *J. Am. Chem. Soc.* **135**, 17853–17861 (2013).
63. Lasisi, K. H., Yao, W., Xue, Q., Liu, Q. & Zhang, K. High performance polyamine-based acid-resistant nanofiltration membranes catalyzed with 1,4-benzenecarboxylic acid in interfacial cross-linking polymerization process. *J. Membr. Sci.* **640**, 119833 (2021).

Author contributions

W.Q.M.: Writing-conceptualization, data curation, methodology, writing—original draft, writing—review & editing. Q.X.: Methodology, Data curation. J.Y.Z.: Investigation, writing—review & editing. K.S.Z.: Conceptualization, funding acquisition, formal analysis, supervision, writing—review & editing.

Competing interests

The authors declare no competing interests.

Additional information

Supplementary information The online version contains supplementary material available at https://doi.org/10.1038/s41545-024-00320-x.

Correspondence and requests for materials should be addressed to Kaisong Zhang.

Reprints and permissions information is available at http://www.nature.com/reprints

Publisher's note Springer Nature remains neutral with regard to jurisdictional claims in published maps and institutional affiliations.